Article

Slow Relaxation of the Magnetization in Anilato-Based Dy(III) 2D Lattices

Samia Benmansour *[ID], Antonio Hernández-Paredes [ID], María Bayona-Andrés and Carlos J. Gómez-García *[ID]

Departamento de Química Inorgánica, ICMol, Universidad de Valencia, C/Catedrático José Beltrán 2, 46980 Valencia, Spain; antonio.hernandez-paredes@uv.es (A.H.-P.); mbayonaandres@hotmail.com (M.B.-A.)
* Correspondence: sam.ben@uv.es (S.B.); carlos.gomez@uv.es (C.J.G.-G.)

Abstract: The search for two- and three-dimensional materials with slow relaxation of the magnetization (single-ion magnets, SIM and single-molecule magnets, SMM) has become a very active area in recent years. Here we show how it is possible to prepare two-dimensional SIMs by combining Dy(III) with two different anilato-type ligands (dianions of the 3,6-disubstituted-2,5-dihydroxy-1,4-benzoquinone: $C_6O_4X_2^{2-}$, with X = H and Cl) in dimethyl sulfoxide (dmso). The two compounds prepared, formulated as: $[Dy_2(C_6O_4H_2)_3(dmso)_2(H_2O)_2]\cdot2dmso\cdot18H_2O$ (**1**) and $[Dy_2(C_6O_4Cl_2)_3(dmso)_4]\cdot2dmso\cdot2H_2O$ (**2**) show distorted hexagonal honeycomb layers with the solvent molecules (dmso and H_2O) located in the interlayer space and in the hexagonal channels that run perpendicular to the layers. The magnetic measurements of compounds **1**, **2** and $[Dy_2(C_6O_4(CN)Cl)_3(dmso)_6]$ (**3**), a recently reported related compound, show that the three compounds present slow relaxation of the magnetization. In compound **1** the SIM behaviour does not need the application of a DC field whereas **2** and **3** are field-induced SIM (FI-SIM) since they show slow relaxation of the magnetization when a DC field is applied. We discuss the differences observed in the crystal structures and magnetic properties based on the X group of the anilato ligands (H, Cl and Cl/CN) in **1**–**3** and in the recently reported derivative $[Dy_2(C_6O_4Br_2)_3(dmso)_4]\cdot2dmso\cdot2H_2O$ (**4**) with X = Br, that is also a FI-SIM.

Keywords: SMM; SIM; anilato ligands; Dy(III); FI-SIM; honeycomb structure; layered materials

1. Introduction

The last years have witnessed an increasing interest in the search for magnetic materials showing slow relaxation of the magnetization of molecular origin (single-molecule magnets, SMM) [1,2] or due to a single ion (single-ion magnets, SIM) [3,4]. The presence of slow relaxation of the magnetization and hysteresis at low temperature in SMMs is due to the presence of an energy barrier, U_{eff}, for the reversal of the magnetization. This energy barrier depends on the spin ground state of the complexes and on the easy-axis magnetic anisotropy and, accordingly, the search of novel SMMs (and SIMs) with higher blocking temperatures and higher energy barriers relies on the combination of anisotropic transition metals and lanthanoids ions (Ln), with low symmetry ligands [5–8].

Although most of the SMMs and SIMs are discrete metallic complexes with different nuclearities, in recent years, some one-dimensional [9–21], a few two-dimensional [22–34] and very few three-dimensional polymers [13,34–36] with SMM behaviour have also been prepared.

Most of these coordination polymers are formed by Mn(II)/Mn(III) clusters of different nuclearities with SMM behaviour, linked by long bridging ligands that isolate them from the magnetic point of view [9–13,22–25,29]. There are also a few coordination polymers containing 3d/4f clusters [14,15,17,26–28] or lanthanoid ions [20,35], including one- [16,18,19,21], two- [30–34] and three-dimensional [34–36] Dy(III) coordination polymers.

Furthermore, the bridging ligands that provide good isolation from the magnetic point of view may also give rise to additional properties as photo-modulation [21], white light emission [19], photoluminescence [20,35] or even novel magnetic states [29].

Besides the search of SMMs and SIMs, lanthanoids have also been used to prepare coordination polymers and metal-organic frameworks showing interesting properties such as solvent and gas exchange or luminescence [37–39].

In recent years, anilato-derivative ligands (3,6-disubstituted of the 2,5-dihydroxy-1,4-benzoquinone dianion = $C_6O_4X_2^{2-}$, Scheme 1a) have been combined with Ln(III) ions to prepare coordination polymers with interesting optical [40–43] or magnetic properties, including SMMs [33,44–46].
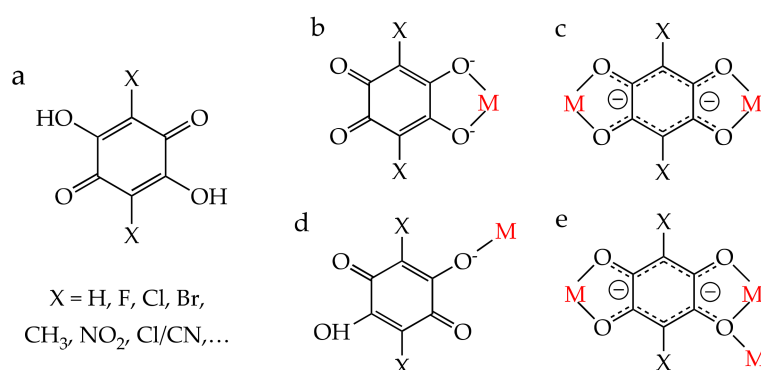
Scheme 1. (**a**) The 3,6-disubstituted anilato derivatives ($H_2C_6O_4X_2$). (**b**–**e**) Some of the coordination modes of the anilato ligands: (**b**) bidentate ($1k^2O,O'$), (**c**) bis-bidentate ($1k^2O,O';2k^2O'',O'''$), (**d**) monodentate ($1kO$) and (**e**) bis-bidentate-monodentate ($1k^2O,O';2k^2O'',O''';3kO''$).

Anilato ligands are very appropriate to construct these materials since: (i) they can act with different coordination modes, such as: bidentate ($1k^2O,O'$), bis-bidentate ($1k^2O,O';2k^2O'',O''$), monodentate ($1kO$), monodentate-bidentate ($1kO;2k^2O',O''$) or other complex modes as ($1k^2O,O';2k^2O'',O''';3kO''$) (Scheme 1b–e) [47,48], (ii) they can connect two different metal atoms (Scheme 1c), giving rise to coordination oligomers and polymers [47], (iii) although they promote tuneable (antiferro)magnetic coupling between transition metal ions [49,50], this coupling is very weak when connecting Ln(III) ions (due to the internal character of the 4f orbitals), providing, thus, a good magnetic isolation, needed to avoid the fast relaxation of the magnetization in order to obtain SMMs and SIMs and (iv) they are equivalent to the well-known oxalato ligand ($C_2O_4^{2-}$) from the topological point of view and they can form similar discrete tris(anilato)metalato complexes [51,52] and extended one-, two- and three-dimensional lattices although with larger channels and cavities [47,48,53–55].

In most of these coordination polymers, the Ln(III) ions are surrounded by three bidentate anilato ligands and complete their octa- or nona-coordination with two or three solvent molecules with a high coordination capacity towards Ln(III) ions [56,57] such as water, dimethyl sulfoxide (dmso), dimethylformamide (dmf), dimetylacetamide (dma), etc. [58–60].

Here we present the synthesis and structure of two novel coordination polymers prepared with Dy(III), dmso and two different anilato ligands: ($C_6O_4X_2$)$^{2-}$, with X = H (2,5-dihydroxy-1,4-benzoquinone = dhbq^{2-}) and X = Cl (chloranilato). These compounds, formulated as [Dy$_2$(C$_6$O$_4$H$_2$)$_3$(dmso)$_2$(H$_2$O)$_2$]·2dmso·18H$_2$O (**1**) and [Dy$_2$(C$_6$O$_4$Cl$_2$)$_3$(dmso)$_4$]·2dmso·2H$_2$O (**2**), crystallize as hexagonal honeycomb layers with dmso and H$_2$O molecules occupying the interlayer space and the hexagonal channels that run perpendicular to the layers. We also present the single-ion magnet behaviour of compounds **1** and **2** and of the closely related compound prepared with the ligand chlorocyananilato (X = Cl/CN): [Dy$_2$(C$_6$O$_4$(CN)Cl)$_3$(dmso)$_6$] (**3**), whose crystal structure has been recently reported by Mercuri et al. [61]. Finally, we present a comparative structural and magnetic study of com-

pounds **1**–**3** and of a forth closely related compound: $[Dy_2(C_6O_4Br_2)_3(dmso)_4]\cdot 2dmso\cdot 2H_2O$ (**4**), also prepared with Dy(III), dmso and an anilato ligand (bromanilato, X = Br), whose structure and magnetic properties have been recently reported by some of us [33,44].

2. Results

2.1. Synthesis

The synthesis of single crystals of the two compounds has been performed using a layering method with $Dy(CH_3COO)_3\cdot 4H_2O$, for **1** and $Dy(NO_3)_3\cdot 5H_2O$, for **2** as precursor salts, with the corresponding anilato acids and dmso as solvent. Surprisingly, when $Dy(NO_3)_3\cdot 5H_2O$ is used instead of $Dy(CH_3COO)_3\cdot 4H_2O$ and/or if NEt_3 is not added to the solution, no single crystals of compound **1** could be obtained. A possible reason may be the lower acidity of H_2dhbq (X = H) compared with the chloranilic (X = Cl) acid. Compound **3** was synthesized as compound **2** but using the precursor salt $KH(C_6O_4(CN)Cl)$.

2.2. X-ray Crystal Structure

2.2.1. Structure of $[Dy_2(C_6O_4H_2)_3(dmso)_2(H_2O)_2]\cdot 2dmso\cdot 18H_2O$ (**1**)

The single crystal X-ray analysis shows that compound **1** crystallizes in the monoclinic *C2/c* space group. The asymmetric unit contains one Dy(III) ion, three halves dhbq^{2-} ligands, one coordinated dmso molecule, one coordinated water molecule, one crystallization dmso molecule and nine disordered crystallization H_2O molecules (Figure 1a), giving rise to the formula: $[Dy_2(C_6O_4H_2)_3(dmso)_2(H_2O)_2]\cdot 2dmso\cdot 18H_2O$.

(**a**)　　　　　　　　　　　　　　　　　(**b**)
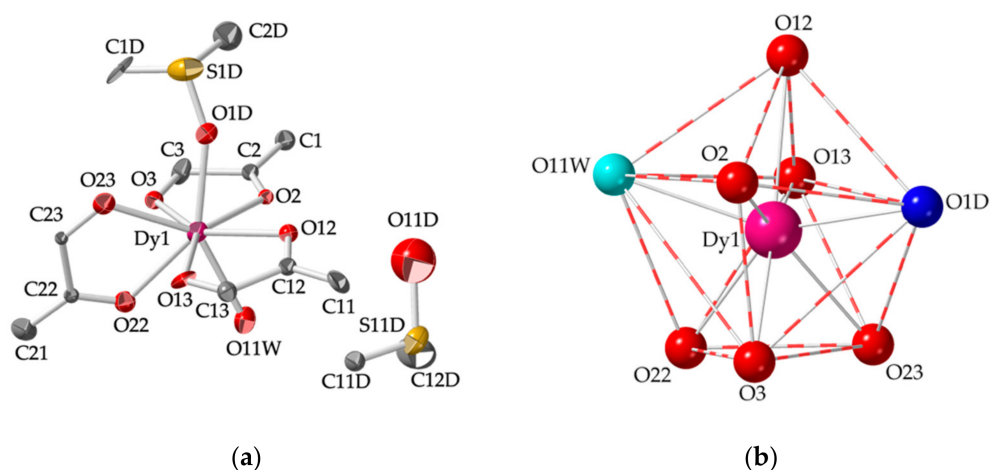
Figure 1. (**a**) Asymmetric unit of compound **1** with the labelling scheme (ellipsoids drawn at 50% probability). H atoms and the crystallization water molecule have been omitted for clarity; (**b**) Coordination environment of the Dy(III) ion in compound **1**. The O atom of the coordinated dmso and water molecules are drawn in dark and light blue, respectively.

The Dy(III) atoms are octa-coordinated by six oxygen atoms from three chelating chloranilato ligands (O2, O3, O12, O13, O22 and O23) and two oxygen atoms from a coordinated dmso molecule (O1D) and from a coordinated water molecule (O11W) with a triangular dodecahedron (TDD-8) coordination geometry [62], as shown by continuous SHAPE measurement analysis (Table S1, Supporting Information) [63–65]. The two O atoms from the coordinated dmso and H_2O molecules are located in *trans* disposition (Figure 1b). The Dy-O bond lengths (Table 1) are similar to those of compound **2** (see below) and of the other Dy-anilato compounds with coordination number eight [44,46]. The Dy-O_{dmso} and Dy-O_{water} bond distances are shorter than the Dy–$O_{anilato}$ ones (Table 1), due to the formation of a five membered chelate ring between the Dy centre and the anilato ligand.

Table 1. Dy-O bond distances (in Å) for compounds **1** and **2**.

Atoms	1	2
Dy1-O2	2.319(11)	2.374(5)
Dy1-O3	2.378(13)	2.382(6)
Dy1-O12	2.437(12)	2.380(6)
Dy1-O13	2.388(12)	2.398(6)
Dy1-O22	2.348(13)	2.375(5)
Dy1-O23	2.325(13)	2.393(6)
Dy1-O1D	2.303(14)	2.319(6)
Dy1-O11W	2.357(14)	-
Dy1-O11D	-	2.293(6)
Dy1-O$_{anilato}$ [1]	2.365	2.384
Dy1-O$_{solvent}$ [2]	2.330	2.306

[1] Average Dy-O$_{anilato}$ distance; [2] Average Dy-O$_{solvent}$ distance.

The three coordinated bis-bidentate dhbq^{2-} ligands connect each Dy(III) ion with its three neighbours (with Dy$\cdots$Dy distances through the dbbq^{2-} bridges of 8.55 and 8.58 Å), giving rise to neutral layers, parallel to the *ab* plane, formulated as [Dy$_2$(C$_6$O$_4$H$_2$)$_3$(dmso)$_2$(H$_2$O)$_2$] and formed by distorted hexagons with a 3,6-gon honeycomb topology (Figure 2a). Each hexagon contains six Dy(III) ions located in the vertices and six dhbq^{2-} ligands forming the sides of the hexagons (Figure 2b). Four anilato rings are oriented parallel to the layer (face-on, *FO*) and the other two are oriented nearly perpendicular to the layer (edge-on, *EO*, Figure 2b), giving rise to the so-called phase IIb [55,58].


(**a**)   (**b**)
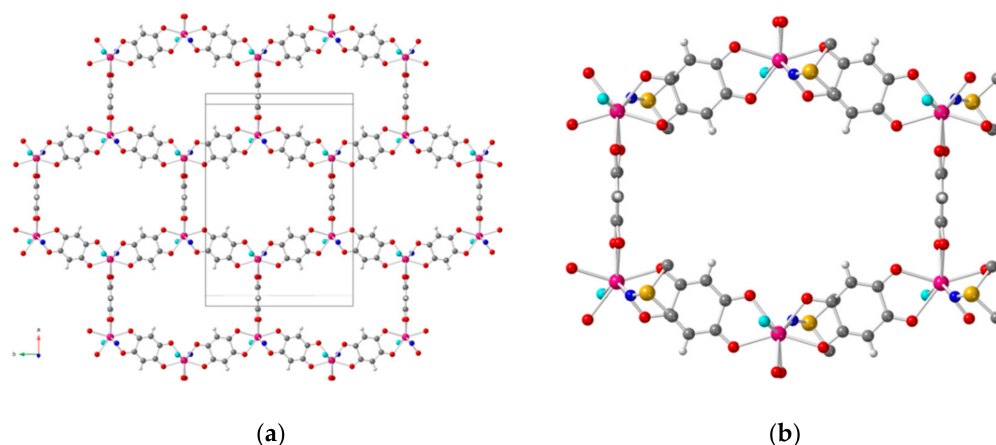
Figure 2. (**a**) Top view of one distorted honeycomb (3,6)-gon layer in **1** (Only the O atom of the coordinated dmso molecules is shown, for clarity); (**b**) View of one hexagonal ring in compound **1**. Colour code: Dy = pink, C = grey, S = yellow, H = white, O$_{anilato}$ = red, O$_{water}$ = light blue, O$_{dmso}$ = dark blue. H atoms (except for the dhbq^{2-} ligands) and crystallization dmso molecules have been omitted for clarity.

Although not very common, distorted hexagonal lattices have already been found in other Ln-anilato compounds with different anilato ligands, solvents and Ln(III) ions [40,41,44,55,58–60,66,67]. In contrast, phase IIb is rather unusual and has only been observed in a few examples of Ln(III) with different anilato ligands (X = Cl, Br, Cl/CN and *t*-Bu) [40,41,44,48–60,67], although it had never been observed with dhbq^{2-} [55]. Therefore, compound **1** is the first example of phase IIb with the ligand dhbq^{2-}.

Two consequences of the distortion of the hexagons are: (i) the deviation from 120° of the Dy–Dy–Dy angles (144.66°, 107.61° and 107.61°) and (ii) the different Dy-Dy distances along the diagonals of the hexagons (17.761, 18.419 and 18.419 Å).

The hexagonal layers are almost planar (Figure 3a), as confirmed by the sum of the three Dy–Dy–Dy angles of 359.88°, very close to 360°, the expected value for a planar

hexagon. The coordinated dmso and water molecules (dark and light blue, respectively, in Figure 3a) are oriented almost orthogonal to the layers pointing towards the interlaminar space, whereas the crystallization dmso molecules (green in Figure 3a) occupy the interlayer space.

(a)   (b)
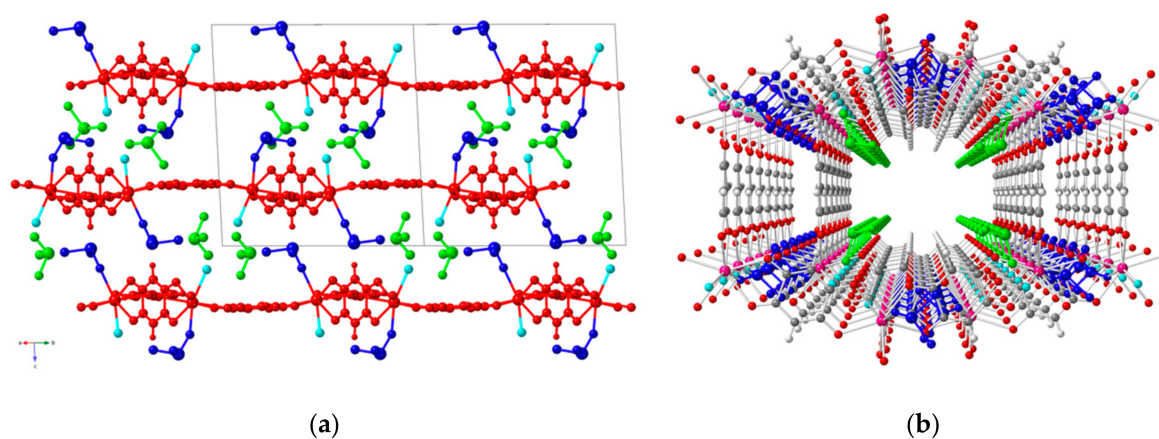
Figure 3. (**a**) Side view of three consecutive layers in compound **1** (in red) showing the coordinated dmso and water molecules (dark and light blue, respectively) and the crystallization dmso molecules (green); (**b**) Perspective view of two rectangular and one hexagonal channels in **1** along the *c* direction showing the crystallization dmso (in green) located in the hexagonal channels.

The layers are packed in a slightly alternating way along the *c* direction (perpendicular to the layers), giving rise to the formation of small empty rectangular channels together with large hexagonal channels along the *c* direction (Figure 3b). The large hexagonal channels contain the crystallization dmso molecules and the disordered crystallization H_2O molecules. The MASK analysis of these hexagonal channels shows that they represent ca. 39% of the unit cell volume and contain 18 H_2O molecules per hexagon (i.e., $[Dy_2(C_6O_4H_2)_3(dmso)_2(H_2O)_2]$), although the low quality of the crystal precludes the exact determination of the location of the water molecules.

2.2.2. Structure of $[Dy_2(C_6O_4Cl_2)_3(dmso)_4]\cdot2dmso\cdot2H_2O$ (**2**)

The single crystal X-ray analysis shows that compound **2** crystallizes in the triclinic *P*-1 space group. The asymmetric unit contains one Dy(III) ion, three halves chloranilato ligands, two coordinated dmso molecules and one dmso and one crystallization H_2O molecules (Figure 4a), resulting in the formula: $[Dy_2(C_6O_4Cl_2)_3(dmso)_4]\cdot2dmso\cdot2H_2O$.

The Dy(III) atoms are octa-coordinated by six oxygen atoms from three chelating chloranilato ligands (O2, O3, O12, O13, O22 and O23) and two oxygen atoms (O1D and O11D) from two coordinated dmso molecules. Continuous SHAPE measurement analysis [64,65] indicates that the coordination geometry around the Dy(III) ion is also a triangular dodecahedron (TDD-8, Table S1, Supporting Information) [62] with the two O atoms from the dmso molecules in *trans* disposition (Figure 4b). The Dy-O bond lengths (Table 1) are similar to those of compound **1** and of the other Dy-anilato compounds with the same coordination number [44,46]. As observed in compound **1**, the Dy-O$_{dmso}$ bond distances are shorter than the Dy–O$_{anilato}$ ones, due to the chelating coordination mode of the chloranilato ligands (Table 1).

The three coordinated bis-bidentate chloranilato ligands connect each Dy(III) with three other Dy(III) ions (with Dy···Dy distances through the chloranilato bridges of 8.65, 8.69 and 8.63 Å), giving rise to neutral distorted hexagonal layers with the classical 3,6-gon honeycomb topology formulated as $[Dy_2(C_6O_4Cl_2)_3(dmso)_4]$ (Figure 5a). The hexagons are formed by six Dy(III) ions and six chloranilato ligands located in the vertices and sides of the hexagons, respectively. Four of the six anilato rings are parallel to the layer (face-on orientation, *FO*) whereas the other two are perpendicular to the layers (edge-on

orientation, *EO*, Figure 5b). This orientation of the anilato rings gives rise to the so-called phase IIb [55,58]. This phase IIb with chloranilato has only been reported for Gd(III) and Eu(III) with H_2O as solvent [58] and for Er(III) with H_2O, dimethylformamide (dmf) and dmso [60], but never with Dy(III). Therefore, compound **2** is the first example of phase IIb with Dy(III) and chloranilato.


(**a**)   (**b**)
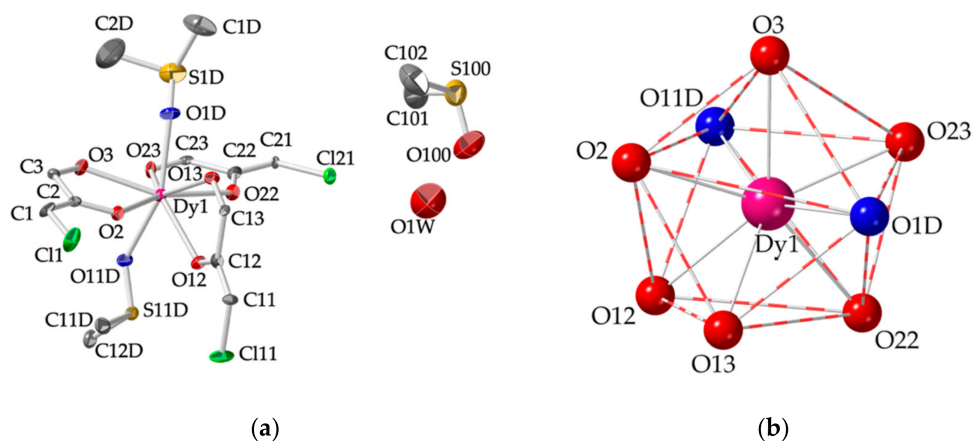
Figure 4. (**a**) Asymmetric unit of compound **2** with the labelling scheme (ellipsoids drawn at 50% probability). H atoms have been omitted for clarity; (**b**) Coordination environment of the Dy(III) ion in compound **2**. O atoms of the coordinated dmso are drawn in dark blue.

(**a**)   (**b**)
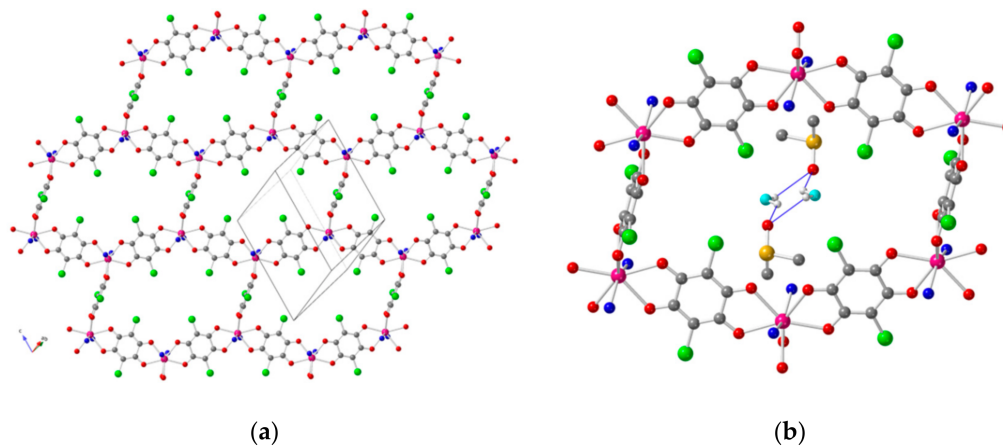
Figure 5. (**a**) Top view of one distorted honeycomb (3,6)-gon layer in **2**; (**b**) View of one hexagonal ring in compound **2**. Thin blue lines represent the H-bonds between the water molecules and the O atoms of the crystallization dmso molecules. Colour code: Dy = pink, C = grey, S = yellow, Cl = green, $O_{anilato}$ = red, O_{water} = light blue, O_{dmso} = dark blue. Only the O atom of the coordinated dmso molecules is shown. H atoms and crystallization dmso molecules (only in (**a**)) have been omitted for clarity.

As in compound **1**, the distortion of the hexagons gives rise to different Dy-Dy-Dy angles (141.78°, 122.36° and 94.87°) and Dy-Dy distances along the diagonals of the hexagons (14.115, 16.606 and 20.247 Å).

The hexagonal layers are almost planar (the sum of the three Dy-Dy-Dy angles is 358.92°, Figure 6a). The coordinated dmso molecules are oriented almost orthogonal to the layers pointing towards the interlaminar space (dark blue in Figure 6a). The crystallization dmso molecules are located in the interlayer space (green in Figure 6a) whereas the water molecules (light blue in Figure 6a) are located very close to the hexagonal plane, in the hexagonal cavities, forming H-bonds with the O atoms of the crystallization dmso molecules (Figure 5b) with O···O distances of 2.865 and 2.963 Å [68].
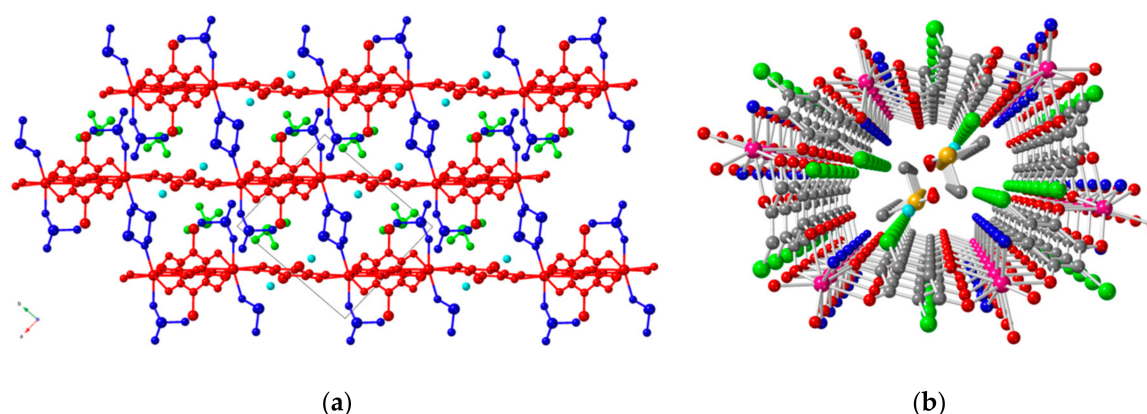
Figure 6. (**a**) Side view of three consecutive layers in **2** (in red) showing the coordinated dmso molecules (dark blue), the crystallization dmso molecules (green) and the crystallization water molecules (ligh blue); (**b**) Perspective view of one hexagonal channel in **2** along the *b* direction showing the crystallization dmso and water molecules located in the channels. Colour code in **b**: Dy = pink, C = grey, S = yellow, Cl = green, $O_{anilato}$ = red, O_{water} = light blue, O_{dmso} = dark blue. H atoms have been omitted for clarity.

A final interesting aspect of the structure of compound **2** is the formation of an eclipsed packing of the layers along the *b* direction. This packing gives rise to hexagonal channels along the *b* direction that contain the crystallization dmso and water molecules (Figure 6b).

3. Discussion

*3.1. Structural Comparison of Compounds [Dy$_2$(C$_6$O$_4$H$_2$)$_3$(dmso)$_2$(H$_2$O)$_2$]·2dmso·18H$_2$O (**1**), [Dy$_2$(C$_6$O$_4$Cl$_2$)$_3$(dmso)$_4$]·2dmso·2H$_2$O (**2**), [Dy$_2$(C$_6$O$_4$(CN)Cl)$_3$(dmso)$_6$] (**3**) and [Dy$_2$(C$_6$O$_4$Br$_2$)$_3$(dmso)$_4$]·2dmso·2H$_2$O (**4**)*

Besides compounds **1** and **2**, there are two, very recently reported compounds, also prepared with dmso, containing Dy(III) and chlorocyananilato (X = Cl/CN) or bromanilato (X = Br) ligands with similar 3,6-gon lattices. These compounds are: $[Dy_2(C_6O_4(CN)Cl)_3(dmso)_6]$ (**3**) [61] and $[Dy_2(C_6O_4Br_2)_3(dmso)_4]·2dmso·2H_2O$ (**4**) [44]. Compounds **1**–**4** show SIM behaviour (see below), although it has only been very recently reported in compound **4** [33]. Besides the X group in the anilato ligand and the number of crystallization solvent molecules, the main difference among compounds **1**–**4** is the number and type of co-ordinated solvent molecules: one H_2O and one dmso in **1**, two dmso molecules in **2** and **4** and three dmso molecules in **3**. Therefore, the main difference is the nona-coordination of the Dy(III) ions in **3** vs. their octa-coordination in **1**, **2** and **4**.

Interestingly, a similar change in the coordination number (from nine to eight), has recently been observed in the related series $[Ln_2(C_6O_4Br_2)_3(dmso)_n]·2dmso·mH_2O$ with n/m = 6/0 for Ln = La-Gd and n/m = 4/2 for Ln = Tb–Tm [44]. Nevertheless, in this series the change in the coordination number is easy to explain based on the size of the Ln(III) ions. Thus, the smaller Ln(III) ions (from Tb to Tm) are octa-coordinated whereas the larger ones (from La to Gd) are nona-coordinated. Another similar change in the coordination number has been observed in two closely related series formulated as $[Er_2(C_6O_4Cl_2)_3(L')_n]·G$ and $[Er_2(C_6O_4Br_2)_3(L')_6]·G$, prepared with the same lanthanoid ion (Er) and chloranilato (X = Cl) or bromanilato (X = Br). In the chloranilato series the coordination number is eight (n = 4) when the solvent molecule is large (L' = formamide = fma, dimethylformamide = dmf or hexamethylphosphormamide = hmpa) whereas it is nine (n = 6) when the coordinating solvent molecules are small (L' = H_2O, dmso or dimethylacetamide = dma) [60]. In the bromanilato series the coordination number is also eight for the larger solvent molecule (L' = dmso) but it is nine when the solvent molecules are smaller (L' = H_2O and dmf) [59]. In these two Er(III)-containing series, the change in the coordination number is attributed to a change in the size and/or steric hindrance of the solvent molecules.

Albeit, in compounds **1**–**4**, the change in the coordination number when passing from compounds **1**, **2** and **4** (with coordination number of eight) to compound **3** (with coordination number of nine), has to be attributed to the change in the X group (X = H, Cl, Cl/CN and Br in **1**–**4**, respectively) since the Ln(III) ion and the coordinated solvent molecules are the same (except in compound **1** where a dmso molecule has been replaced by an H_2O molecule).

Moreover, a detailed study of compound **3**, performed by Mercuri et al. [61], shows that this compound may crystallize as two different phases when recrystallized from dmso: (i) a double square (3,8)+(3,4)-2D lattice formulated as $[Dy_2(C_6O_4(CN)Cl)_3(dmso)_6]\cdot 7H_2O$ (**3′**) and (ii) a rectangular brick-wall (3,6)-2D lattice formulated as $[Dy_2(C_6O_4(CN)Cl)_3(dmso)_6]$ (**3**). Both phases contain nona-coordinated Dy(III) ions with a capped square antiprismatic coordination geometry (CSAPR-9) formed by three bidentate chlorocyananilato ligands and three coordinated dmso molecules. The only difference is the distortion of the CSAPR-9 geometry, which is more important in compound **3**, as clearly shown by the continuous SHAPE measurement analysis, with values of 0.114 and 0.500 for the CSAPR-9 geometry in **3′** and **3**, respectively [64,65]. From the synthetic point of view, the only differences are the concentration of the recrystallization solution (0.33 mg/mL in **3** vs. 1 mg/mL in **3′**) and the recrystallization time (2 weeks in **3** vs. 2–5 days in **3′**), suggesting that **3′** is the kinetic phase whereas **3** is the thermodynamic one. In our case, we obtained compound **3** after two weeks (see Experimental Section) and, as expected, we have obtained the thermodynamic phase (compound **3**). Although the synthesis of **3** and **3′** indicates that the synthetic conditions are a key factor in determining the final structure, it does not explain why the Dy(III) ions in compounds **3** and **3′** are nona-coordinated but they are octa-coordinated in compounds **1**, **2** and **4**.

In order to answer this question, we have, therefore, to focus on the anilato ligands. In compounds **3** and **3′** the Cl and CN groups exert a strong electron withdrawing effect on the anilato ring that reduces the electron density on the coordinating O atoms, resulting in weaker (and longer) Dy-$O_{anilato}$ bonds. These longer Dy-O bonds allow the coordination of up to three dmso molecules. In contrast, in compounds **1**, **2** and **4**, the electron withdrawing effect is smaller, resulting in stronger (and shorter) Dy-$O_{anilato}$ bonds that reduce the available space around the Dy(III) ions and preclude the coordination of a third dmso molecule. This assumption is confirmed by the much shorter average Dy-$O_{anilato}$ bond distances in compounds **1**, **2** and **4** (2.365, 2.384 and 2.384 Å, respectively) than in compounds **3** and **3′** (2.457 and 2.453 Å, respectively). A similar effect was observed in the chloranilato and bromanilato 2D honeycomb heterometallic lattices with Mn(II) and Cr(III): $[MnCr(C_6O_4Cl_2)_3(H_2O)]^-$ and $[MnCr(C_6O_4Br_2)_3]^-$, where the more electron withdrawing X group (Cl) leads to a higher coordination number (seven) and the less electron withdrawing X group (Br) results in a lower coordination number (six) [49].

The key role in the final structure of the coordination geometry around the Dy(III) ion observed in **3** and **3′**, is further confirmed in compounds **1**, **2** and **4**. Thus, compounds **1**, **2** and **4** present similar distorted hexagonal honeycomb structures whereas compound **3** presents a brick-wall structure with almost rectangular cavities. These differences in the shape of the cavities are directly related to the orientation of the anilato ligands in the coordination polyhedra of the Dy(III) ions in compounds **1**–**4** (Figure 7a–d). Thus, in compounds **1**, **2** and **4** the spatial orientation of the anilato ligands is the same and, consequently, they present similar distorted hexagonal layers. Furthermore, compounds **2** (X = Cl) and **4** (X = Br) are isostructural [44]. In contrast, compound **3** shows a different coordination number and geometry (although with a similar spatial disposition of the three anilato ligands) and, accordingly, shows a much more distorted structure although with the same 3,6-gon topology (Figure 7e–h).
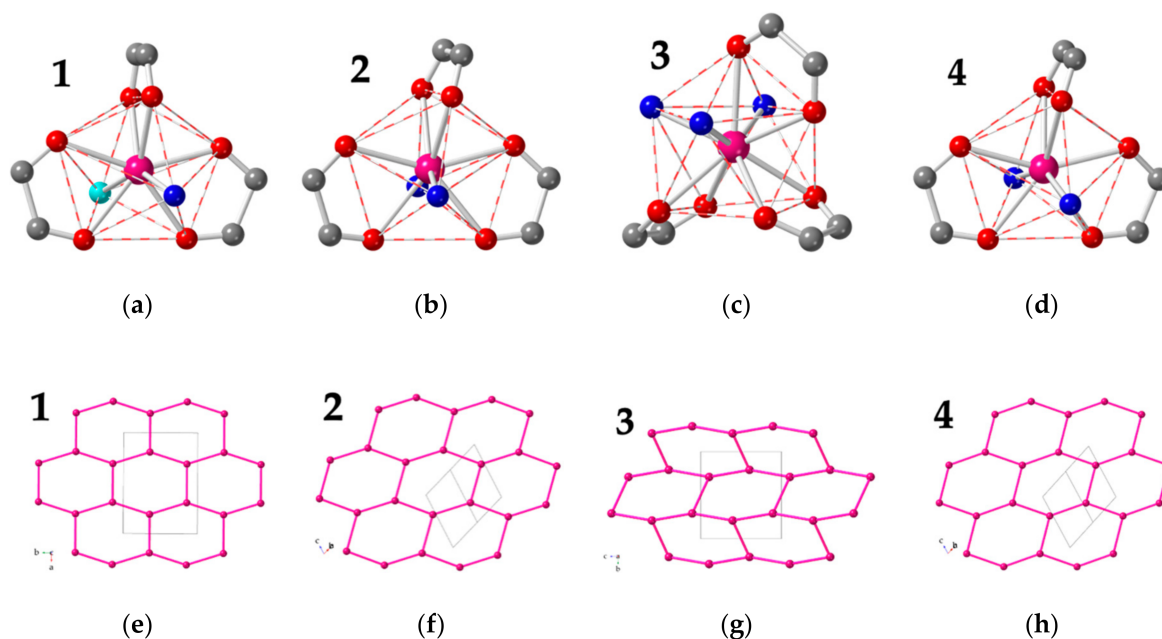
Figure 7. (**a**–**d**) Coordination polyhedra of compounds **1**–**4**. Colour code: Dy = pink, C = grey, $O_{anilato}$ = red, O_{water} = light blue, O_{dmso} = dark blue. (**e**–**h**) Schematic view of the layers in compounds **1**–**4**. Only the Dy atoms are shown for clarity. The pink lines represent the anilato bridges.

### 3.2. Magnetic Properties of Compounds **1**–**4**

Although the DC magnetic properties of compound **3** have already been reported [61], we include them only for comparative purposes. In contrast, AC measurements of compound **3** have not been reported yet and, therefore, here we will show a detailed study of the AC magnetic properties of this compound, as well as those of compounds **1** and **2**.

The DC magnetic measurements of compounds **1**–**3** show very similar behaviours for the three compounds. The product of the molar magnetic susceptibility per two Dy(III) ions times the temperature ($\chi_m T$) is around 28.5 cm^3 K mol^{-1} at room temperature for the three compounds and shows a smooth decrease when the samples are cooled to reach values of ca. 21.0, 23.5 and 22.5 cm^3 K mol^{-1} at 2 K for **1**−**3**, respectively (Figure S1a, Supporting Information). The room temperature value is close to the expected one for two isolated Dy(III) ions with a $^6H_{15/2}$ ground multiplet and g = 4/3 and the thermal behaviour is also the expected one for magnetically isolated Dy(III) ions and is attributed to the depopulation of the excited sublevels appearing due to the ligand field [69]. The magnetic isolation of the Dy(III) ions is not surprising and has been observed in other compounds with Ln(III) ions connected through bis-bidentate anilato ligands [40,44,59,60,70,71].

The isothermal magnetization at 2 K also shows the expected behaviour for isolated Dy(III) ions with a rapid increase at low fields and a smooth and linear increase at high fields with a value of ca. 6 μ_B per Dy(III) ion at high fields (Figure S1b, Supporting Information) and shows saturation values close to those observed in other Dy(III) compounds with isolated Dy(III) ions [72,73].

The AC magnetic measurements for compound **1** show slow relaxation of the magnetization at low temperatures with and without an applied DC field. Thus, the frequency dependence of the in–phase (χ'_m) and out–of–phase (χ''_m) signals for compound **1** with no DC field shows a decrease in χ'_m (Figure S2a, Supporting Information) and an increase in χ''_m at high frequencies (Figure 8a) with no maximum below 10 kHz, indicative of slow relaxation of the magnetization at low temperatures. Although the inflexion point in χ'_m and the maximum in χ''_m are not reached at 10 kHz, we can observe that the maximum slope in χ''_m is located near 2–3 kHz and, accordingly, we can assume that the maximum in χ''_m must be located slightly above 10 kHz, although the exact position cannot be determined

with our set of data. Despite this uncertainty, we have fitted both signals, χ'_m and χ''_m, with the Debye model (solid lines in Figure S2a and Figure 8a) to obtain the corresponding relaxation times in the temperature range 1.9–4.0 K.
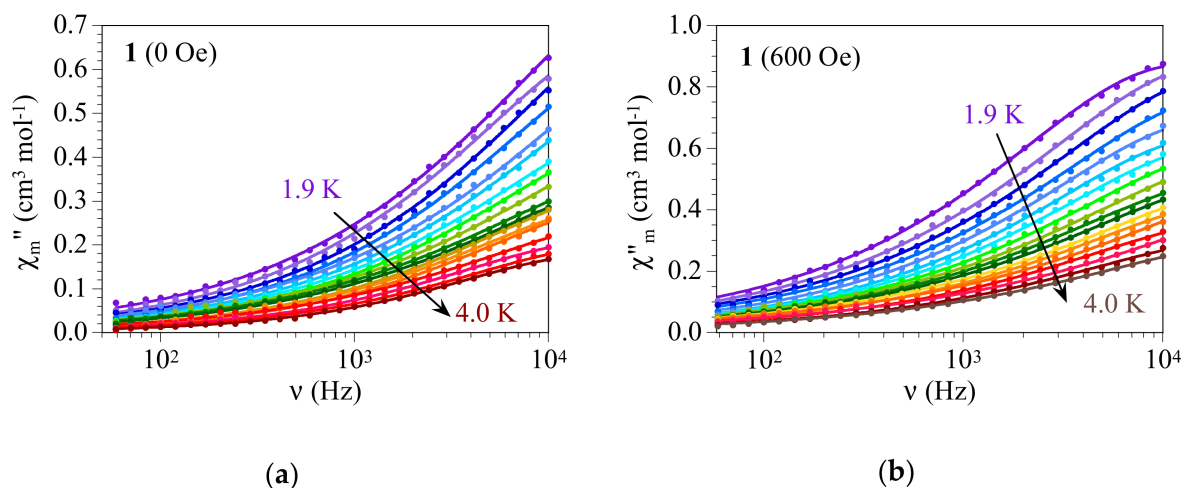
Figure 8. (**a**) Frequency dependence of χ''_m for compound **1** with $H_{dc} = 0$ Oe in the temperature range 1.9–4.0 K; (**b**) Frequency dependence of χ''_m for compound **1** with $H_{dc} = 600$ Oe in the temperature range 1.9–4.0 K. Solid lines are the best fit to the Debye model.

When a DC magnetic field is applied at 1.9 K, the χ''_m signal increases with increasing the DC field and reaches a maximum at around 600 Oe at high frequencies (that shifts to higher fields for lower frequencies, Figure S3, Supporting Information). The study of the frequency dependence at 1.9 K for different DC fields (Figure S4, Supporting Information) shows that the intensity of χ''_m increases as the DC field increases and reaches a maximum value at ca. 600 Oe. For all DC fields the maximum of χ''_m appears above 10 kHz and, therefore, the fit of the frequency dependence of χ''_m to a Debye model is not very precise. Nevertheless, we observe that the relaxation time (τ) presents a maximum near 600 Oe and that the field dependence of τ follows the expected variation with n = 4 for Kramers ions (Figure S5, Supporting Information) [74]:

$$\tau^{-1} = \text{ATH}^n + \frac{B_1}{1 + B_2 H^2} + D \tag{1}$$

Accordingly, we have performed AC measurements at different temperatures and frequencies with a DC field of 600 Oe. These measurements show again frequency-dependent χ'_m and χ''_m signals (Figure S2b and Figure 8b) very similar behaviour to those performed with no applied DC field that can also be fitted to the Debye model (solid lines in Figure S2b and Figure 8b).

The Cole-Cole plots (χ''_m vs. χ'_m, Figure S6, Supporting Information) show a fragment of a semicircle, confirming the presence of slow relaxation of the magnetization.

For compound **2** the AC measurements with no applied DC field do not show any AC signal, probably due to the presence of a fast quantum tunnelling process for $H_{DC} = 0$ Oe. Albeit, when a DC field is applied, we can observe the appearing of χ'_m and χ''_m signals at low temperatures with a maximum χ''_m signal for a DC field of ca. 1000 Oe. (Figure S7, Supporting Information). The frequency dependence of χ''_m at 1.9 K with different applied DC fields for compound **2** shows a clear maximum in χ''_m whose intensity increases as the DC field increases and reaches a maximum intensity at around 900–1000 Oe (Figure S8, Supporting Information). The relaxation times obtained with the fit of χ''_m to de Debye model show a maximum at ca. 1000 Oe (0.1 T, Figure S9, Supporting Information) and follow the expected field dependence (Equation (1)). Accordingly, we have performed AC measurements at different frequencies and temperatures with an applied DC field of

1000 Oe (Figure 9). These measurements show an inflexion in χ'_m that shifts to higher frequencies as the temperature increases (Figure 9a) and a maximum in χ''_m that also shifts to higher frequencies with increasing temperature (Figure 9b) that can be well reproduced with the Debye model (solid lines in Figure 9). The Cole-Cole plot of compound **2** with H_{DC} = 1000 Oe also shows a semi-elliptical curve although now we can see a much larger fragment at low temperatures (Figure S10, Supporting Information).

(a)

(b)
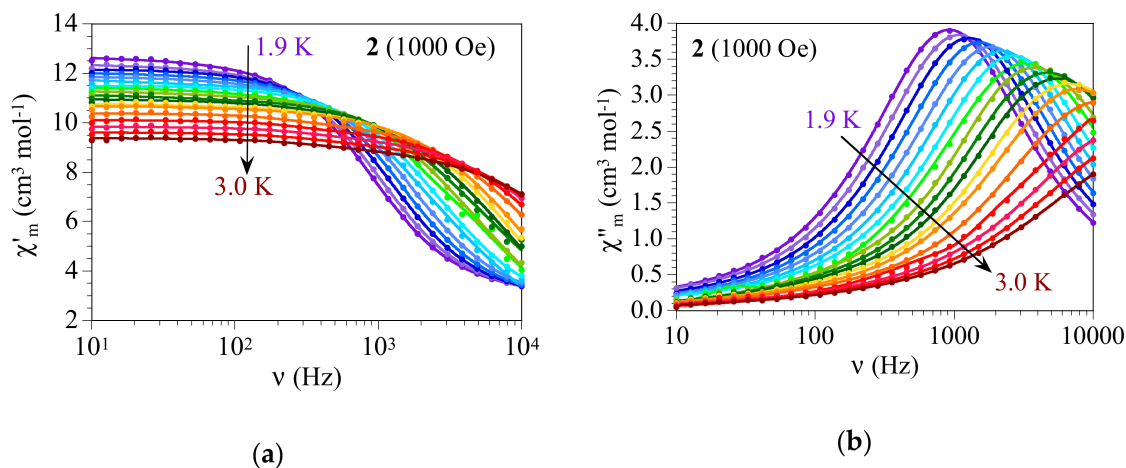
Figure 9. (**a**) Frequency dependence of χ'_m for compound **2** with H_{dc} = 1000 Oe in the temperature range 1.9–3.0 K; (**b**) Frequency dependence of χ''_m for compound **2** with H_{dc} = 1000 Oe in the temperature range 1.9–3.0 K. Solid lines are the best fit to the Debye model.

Finally, compound **3** also shows slow relaxation of the magnetization although, as can be seen in the field dependence of χ''_m for compound **3** at 1.9 K (Figure S11, Supporting Information), we need to apply a DC field to observe the SIM behaviour, probably, as in **2**, due to the presence of a fast quantum tunnelling process for H_{DC} = 0 Oe. Since the maximum in the χ''_m signal is observed for fields of ca. 1000 Oe, we have performed AC measurements at different frequencies and temperatures with H_{DC} = 1000 Oe. These measurements suggest the presence of an inflexion point in the frequency dependence of χ'_m above 10 kHz (Figure 10a). The χ''_m signal shows an increase at high frequencies although no maximum is observed below 10 kHz (Figure 10b). Although, as in compound **1**, we do not observe the inflexion point in χ'_m nor the maximum in χ''_m, we have fitted the frequency dependence of χ'_m and χ''_m to a Debye model to obtain approximate relaxation times at very low temperatures.

(a)

(b)
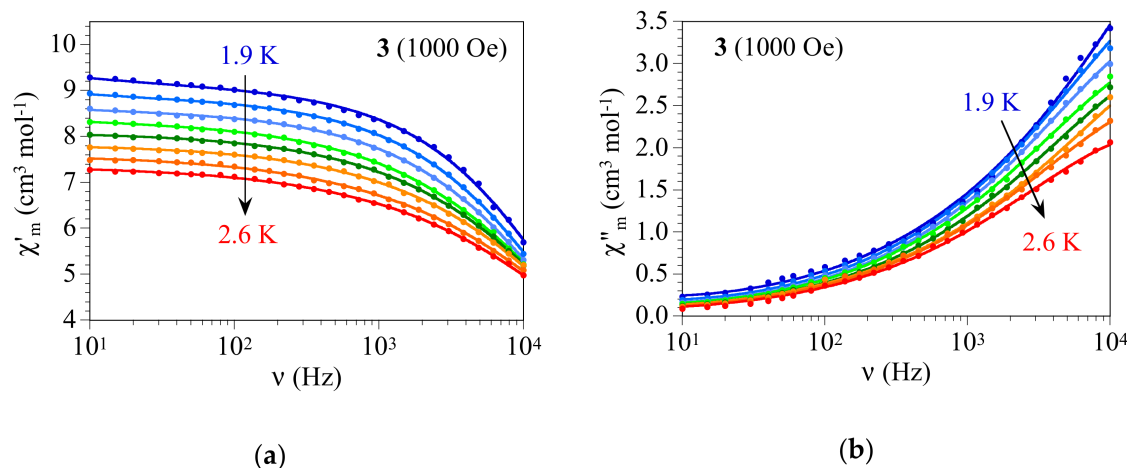
Figure 10. Frequency dependence of χ'_m (**a**) and χ''_m (**b**) for compound **3** with H_{dc} = 1000 Oe in the Table 1. 9–2.6 K. Solid lines are the best fit to the Debye model.

A further confirmation of the presence of a relaxation process is provided by the Cole-Cole plot that shows a semicircle that can be well reproduced with the Debye model although we only observe a small fraction of the semicircle (Figure S12, Supporting Information).

The Arrhenius plots of the relaxation times in compounds **1–3** (Figure 11) show an almost horizontal straight line for **1** when $H_{DC} = 0$ Oe and a curvature for $H_{DC} = 600$ Oe. In compounds **2** and **3** the relaxation times for $H_{DC} = 1000$ Oe also show a curvature (very slight in **3** and more pronounced in compound **2**).
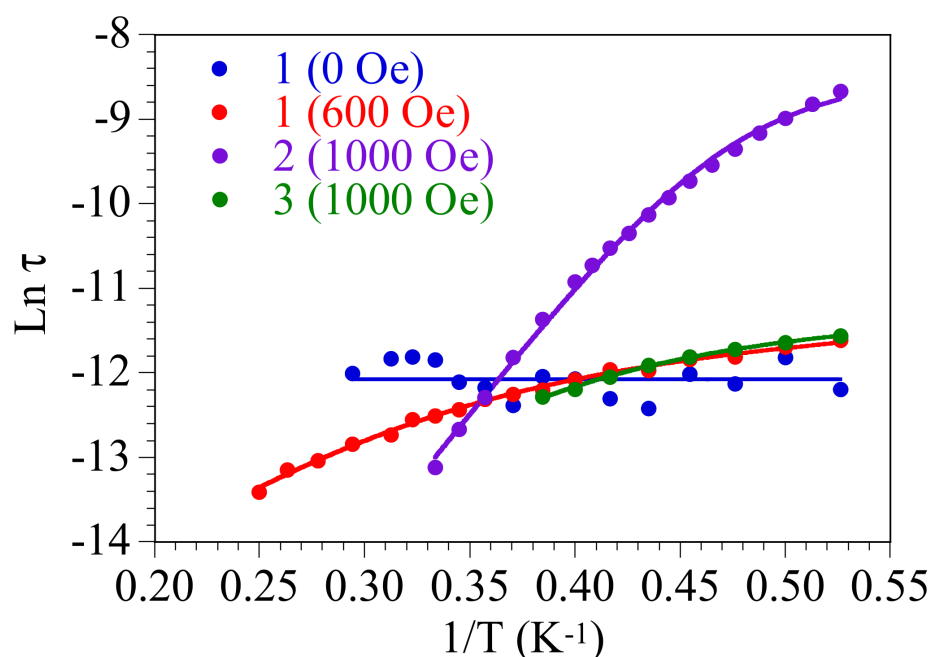
Figure 11. Arrhenius plot of the relaxation times for compound **1** with $H_{DC} = 0$ and 600 Oe, and for compounds **2** and **3** with $H_{DC} = 1000$ Oe. Solid lines are the best fit to the general model (Equation (2)) with different terms (see text and Table 2).

Table 2. Magnetic parameters for the relaxation processes in compounds **1–4**.

| Compound	X	H (Oe)	Mechanisms	τ_{QT} (s)	τ_0 (s)	U_{eff} (K)	AH^2 (K^{-1})
1	H	0	QT	$5.7(3) \times 10^{-6}$	-	-	-
1	H	600	O + D	-	$3.5(9) \times 10^{-8}$	17.1(9)	$5.8(2) \times 10^4$
2	Cl	1000	O + D	-	$6(1) \times 10^{-11}$	31.5(7)	$2.8(2) \times 10^3$
3	Cl/CN	1000	O + D	-	$4.6(5) \times 10^{-9}$	21(3)	$5.3(2) \times 10^4$
4	Br	1000	O + D + QT	$8.5(4) \times 10^{-7}$	$2.0(1) \times 10^{-9}$	22.8(4)	$1.0(3) \times 10^5$

In order to fit the relaxation times, we have used the general model including all the possible mechanisms: quantum tunnelling (QT, first term), direct (D, second term), Raman (R, third term) and Orbach (O, fourth term) (Equation (2)) [75]:

$$\tau^{-1} = \tau_{QTM}^{-1} + AH^2T + CT^n + \tau_0^{-1} \exp\left(\frac{-U_{eff}}{k_BT}\right) \tag{2}$$

For compound **1** with $H_{DC} = 0$ Oe, despite the uncertainty, we observe an approximately temperature independent behaviour of the relaxation time (Figure 11), suggesting that only the quantum tunnelling mechanism is operative at very low temperatures. Accordingly, we have fitted the relaxation times considering only a quantum tunnelling term (see Table 2). In contrast, when a DC field is applied, the relaxation of the magnetization in compounds **1–3** follow direct and thermally activated Orbach mechanisms

(Table 2) with activation energies in the range 17.1–31.5 K, similar to the activation energies observed in the very few reported examples of 2D lattices with Dy and anilato ligands: [Dy$_2$(C$_6$O$_4$Br$_2$)$_3$(H$_2$O)$_6$]·8H$_2$O (9.6 K) [33], [Dy$_2$(C$_6$O$_4$Br$_2$)$_3$(dmf)$_6$] (11.4 and 36 K) [33] and [Dy$_{0.04}$Eu$_{1.96}$(C$_6$O$_4$Br$_2$)$_3$(dmso)$_6$]·2dmso (40.9 K) [45]. Of course, in compounds **1** and **3** the obtained values have to be considered with caution, given the uncertainty in the fit of the AC signals to the Debye model.

As mentioned above, the DC magnetic properties of compounds **1** and **2** are very similar and also similar to those of compounds **3** and **4** [33,61]. The only differences are, therefore, observed in the AC magnetic properties (Figure 12).
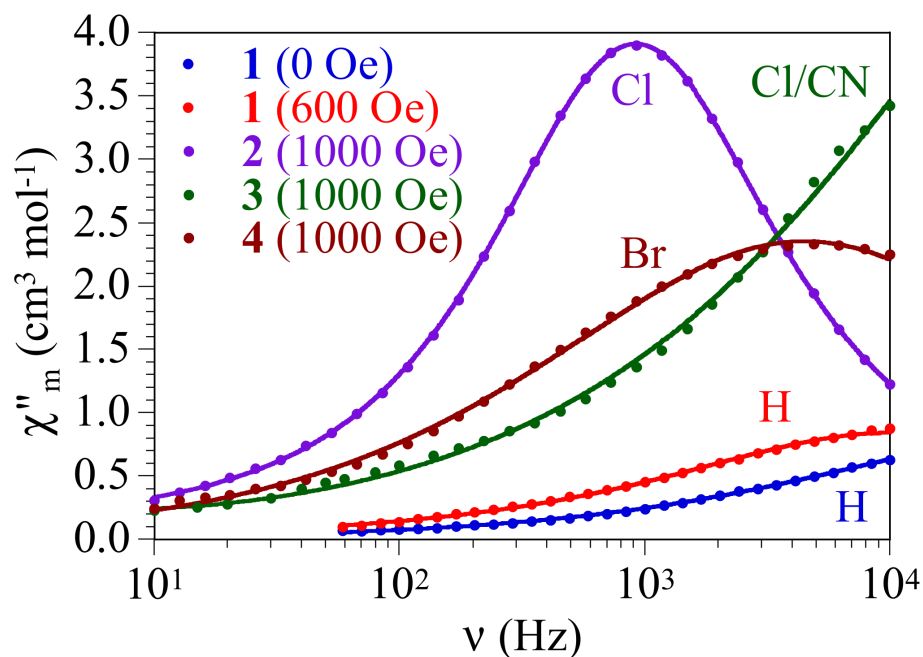
Figure 12. Frequency dependence of χ''_m for compounds **1** (X = H; H$_{dc}$ = 0 and 600 Oe), **2** (X = Cl; H$_{dc}$ = 1000 Oe), **3** (X = Cl/CN; H$_{dc}$ = 1000 Oe) and **4** (X = Br; H$_{dc}$ = 1000 Oe) at 1.9 K. Solid lines are the best fit to the Debye model.

Note that the AC magnetic properties of the X = Br derivative (compound **4**) have been recently reported by some of us [33] and, therefore, we include this compound here to compare with **1**–**3**.

The main difference between compounds **1**–**4** is the presence of slow relaxation in compound **1** with no applied DC field. This relaxation is, nevertheless, quite fast since the maximum of the frequency dependence of χ''_m cannot be observed below 10 kHz and, most probably, it follows a temperature-independent quantum tunnelling mechanism. A possible reason to explain this different behaviour may be the presence of a more anisotropic coordination environment of the Dy(III) ions in compound **1** (formed by three bidentate anilato ligands, one dmso and one water molecule) compared to compounds **2**–**4**, where the coordination environment only contains three bidentate anilato ligands and two (in **2** and **4**) or three (in **3**) dmso molecules (Figure 7a–d).

When a DC field is applied in compounds **1**–**3** the quantum tunnelling mechanism is cancelled and the magnetization relaxes through direct and Orbach mechanisms. Albeit, the activation energies, U$_{eff}$, and the relaxation times, τ_0, show some differences (Table 2). These differences may be attributed to: (i) structural effects due to changes in the coordination of the Dy(III) ions and/or (ii) electronic effects, due to changes in the donor capacity of the anilato ligands as a consequence of the different electron withdrawing capacity of the X group.

On one hand, the structural effect can be approximately quantified by the distortion from the ideal TDD-8 coordination geometry of the Dy(III) ions since they all show the same connectivity and the same disposition of the bridging ligands and solvent molecules (Figure 7). Continuous shape analysis (Table S1, Supporting Information) shows distortion values from ideal TDD-8 geometry of 0.902 in **1**, 1.208 in **2** and 1.079 in **4** [33]. On the other hand, the electronic effect can be quantified by the electronegativity of the X group of the anilato ligand (H in **1**, Cl in **2** and Br in **4**).

Although there are only three compounds to establish a correlation, we observe an almost linear dependence of both parameters (Ln τ_0 and U_{eff}) with both the distortion parameter and with the electronegativity of the X group. Thus, Ln τ_0 decreases (blue line in Figure S13) and U_{eff} increases (blue line in Figure S14) as the distortion parameter increases. The same trend is observed for the electronegativity of the X group: Ln τ_0 decreases (red line in Figure S13) and U_{eff} increases (red line in Figure S14) as the electronegativity increases.

Although we need to synthesize and characterize other similar examples with Dy(III) and different anilato ligands to confirm these trends, we observe that the larger the distortion of the coordination polyhedron around the Dy(III) ion, the higher U_{eff} and the lower τ_0. On the other side, when the electron withdrawing capacity of X increases, the ligand-Dy interaction decreases, resulting in the same effect: an increase of U_{eff} and a decrease of τ_0. These trends agree with the idea that the larger the distortion and the weaker the metal-ligand interaction, the larger the anisotropy.

4. Materials and Methods

4.1. Synthesis of Compounds **1–3**

All the chemicals are commercially available and were used as received without further purification. The reactions were performed in open air. The potassium acid salt of the chlorocyananilato ligand, $KH(C_6O_4(CN)Cl)$, was prepared following the method reported in the literature [76].

4.1.1. Synthesis of $[Dy_2(C_6O_4H_2)_3(dmso)_2(H_2O)_2]\cdot2dmso\cdot18H_2O$ (**1**)

Dark pink prismatic single crystals of compound **1** were obtained by carefully layering, at room temperature, a solution of $Dy(CH_3COO)_3\cdot4H_2O$ (0.01 mmol. 3.4 mg) in 2.5 mL of methanol onto a solution of 2,5-dihydroxy-1,4-benzoquinone, $H_4C_6O_4$, (0.01 mmol, 1.4 mg) and triethylamine (0.36 mmol, 50 μL) in 2.5 mL of dmso. The tube was sealed and allowed to stand for about 4 months. Suitable crystals for X-ray diffraction were freshly picked and covered with paratone oil in order to avoid solvent loss to be characterized by single crystal X-ray diffraction. FT-IR (ν/cm^{-1}, KBr pellets): 3432 (m), 2990 (w), 2910 (w), 1522 (vs), 1374 (m), 1262 (m), 1022 (m), 955 (w), 831 (w), 712 (w), 494 (w). This compound losses very quickly in an irreversible way part of the solvent molecules when exposed to air, resulting in a loss of crystallinity that precludes the acquisition of an X-ray powder diffractogram of this compound.

4.1.2. Synthesis of $[Dy_2(C_6O_4Cl_2)_3(dmso)_4]\cdot2dmso\cdot2H_2O$ (**2**)

Pink prismatic single crystals of **2** were obtained by carefully layering, at room temperature, a solution of chloranilic acid, $H_2C_6O_4Cl_2$ (0.02 mmol, 4.2 mg) in 5 mL of methanol onto a solution of $Dy(NO_3)_3\cdot5H_2O$ (0.02 mmol. 8.77 mg) in 5 mL of dmso. The tube was sealed and allowed to stand for about 6 weeks. Suitable crystals for X-ray diffraction were freshly picked and covered with paratone oil in order to avoid solvent loss to be characterized by single crystal X-ray diffraction.

This compound was also obtained in a one-pot synthesis as a polycrystalline sample by adding, drop-wise, a solution of $Dy(NO_3)_3\cdot5H_2O$ (0.1 mmol. 43.9 mg) in 10 mL of dmso to a solution of chloranilic acid, $H_2C_6O_4Cl_2$ (0.15 mmol, 31.5 mg) in 10 mL of dmso at 40 °C. After 30 min stirring at 40 °C the solution was covered and allowed to stand at room temperature. Three days later, a dark purple solid precipitated. The solution was

filtered and air dried. Yield: 45%. FT-IR (v/cm^{-1}, KBr pellets): 3421 (m), 2998 (w), 2918 (w), 1495 (vs), 1381 (s), 1295 (w), 1000 (m), 959 (m), 846 (m), 712 (w), 604 (w), 579 (m), 451 (m).

Phase purity was confirmed by the X-ray powder diffractogram of compound **2** that corresponds with the simulated one from the single crystal X-ray structure (Figure S15, Supporting Information).

4.1.3. Synthesis of $[Dy_2(C_6O_4(CN)Cl_2)_3(dmso)_6]$ (**3**)

This compound was obtained as compound **2** but using $KH(C_6O_4(CN)Cl)$ (0.15 mmol, 35.7 mg) instead of $H_2C_6O_4Cl_2$. After 30 min stirring at 40 °C the solution was covered and allowed to stand at room temperature. Two weeks later, a purple solid precipitated. The solution was filtered and air dried. Yield: 13%. FT-IR (v/cm^{-1}, KBr pellets): 3419 (m), 3000 (w), 2921 (w), 2213 (m), 1520 (vs), 1415 (m), 1002 (m), 958 (m), 861 (m), 713 (w), 612 (m), 482 (w), 445 (m).

The X-ray powder diffractogram of compound **3** corresponds well with the simulated one from the single crystal X-ray structure reported by Mercuri et al. [61] for compound $[Dy_2(C_6O_4(CN)Cl)_3(dmso)_6]$ (Figure S16), confirming the phase purity of this compound.

4.2. X-ray Single Crystal Structure Determination

Suitable crystals of compounds **1** and **2** were freshly picked from the mother liquor, immediately coated with paratone oil, mounted on a mylar loop and then transferred directly to the cold-nitrogen stream for data collection. X-ray data were collected at 120 K using ω scans on a Supernova diffractometer equipped with a graphite-monochromated Enhance (Mo) X-ray source (λ = 0.71073 Å). The program CrysAlisPro (Oxford Diffraction Ltd., Oxfordshire, UK) was used for unit cell determinations, data reduction, scaling and for a multi-scan absorption correction using spherical harmonics implemented in SCALE3 ABSPACK. The structures were solved in the space groups $C2/c$ (for **1**) and P-1 (for **2**) determined by the ShelXT structure solution program using the Intrinsic Phasing solution method [77] and refined by least squares using version 2017/1 of XL [78]. All non-hydrogen atoms were refined anisotropically. Hydrogen atom positions were calculated geometrically and refined using the riding model. Data collection and refinement parameters are provided in Table 3.

Compound **1** shows a positional disorder in one C atom of the coordinated dmso molecule that appears on two close positions (C2D and C2D′, separated by 1.28 Å) that appear with occupancies of 0.75 and 0.25, respectively. In all the drawings only the C2D atom is drawn, since C2D′ is too far (2.125 Å) from the S atom of the dmso molecule. For compound **1**, due to severely disordered solvent molecules, the solvent contributions to the structure factors were taken into account by applying the MASK procedure in the OLEX2 program package [79]. Solvent accessible voids and total electron counts found per cell for **1** are 2033.6 Å^3 (39%) and 692.1, respectively. This is consistent with the presence of ca. 9 H_2O per formula unit (ca. 18 molecules per two Dy ions). Refinement details and explanations are included in the CIF file. CCDC 2054147 and 2054148 contain the crystallographic data of compounds **1** and **2**, respectively.

4.3. X-ray Powder Diffraction

The X-ray powder diffractograms were collected for polycrystalline samples of compounds **2** and **3** filled into a 0.7 mm glass capillary that were mounted and aligned on a Empyrean PANalytical powder diffractometer (Malvern, UK), using CuKα radiation (λ = 1.54177 Å). A total of 3 scans were collected at room temperature in the range 5–40°. The experimental X-ray powder diffractogram of compounds **2** and **3** were compared with the simulated one from the X-ray single crystal structure of compounds **2** and XOYTUD, respectively, reported by Mercuri et al. [61].

Table 3. X-ray crystal data collection for compounds $[Dy_2(C_6O_4H_2)_3(dmso)_2(H_2O)_2]\cdot 2dmso\cdot 18H_2O$ (**1**) and $[Dy_2(C_6O_4Cl_2)_3(dmso)_4]\cdot 2dmso\cdot 2H_2O$ (**2**).

Compound	1	2
CCDC	2054147	2054148
Formula	$C_{13}H_{12}DyO_9S_2$	$C_{15}H_{14}O_{10}DyCl_3S_3$
$\rho_{calc.}$ (g cm^{-3})	1.360	1.934
μ (mm^{-1})	3.026	3.648
Formula weight	538.85	719.29
Color	Dark Pink	Pink
Shape	Prism	Prism
Size	$0.10 \times 0.05 \times 0.02$	$0.14 \times 0.12 \times 0.02$
T (K)	119.6(8)	120(2)
Crystal System	monoclinic	Triclinic
Space group	$C2/c$	P-1
a (Å)	22.339(2)	9.7197(6)
b (Å)	16.2988(14)	10.6161(7)
c (Å)	14.5064(14)	12.7564(7)
α (^{0})	90	78.913(5)
β (^{0})	94.662(8)	73.305(5)
γ (^{0})	90	83.920(5)
V(Å^3)	5264.3(8)	1235.46(14)
Z	8	2
Wavelength (Å)	0.71073	0.71073
Radiation type	MoKα	MoKα
θ_{min} (^{o})	6.04	3.632
θ_{max} (^{o})	50.1	24.070
Mesures Refl.	10245	8103
Independent Refl.	9970	4372
Reflections with I > 2σ(I)	7642	3680
R_{int}	0.0633	0.0413
Parameters	238	301
Restraints	148	6
Largest pick (e$^-$ Å^{-3})	7.30	1.652
Deepest Hole (e$^-$ Å^{-3})	−4.26	−1.549
R$_1$ [a]	0.1184	0.0520
R$_1$ (all data)	0.1396	0.0666
wR$_2$ [b]	0.2946	0.1127
wR$_2$ (all data)	0.3164	0.1248
GooF [c]	1.040	1.116

[a] $R_1 = \Sigma||F_o| - |F_c||/\Sigma|F_o|$; [b] $wR_2 = [\Sigma w(F_o^2 - F_c^2)^2/\Sigma w(F_o^2)^2]^{1/2}$; [c] $GOF = [\Sigma[w(F_o^2 - F_c^2)^2/(N_{obs} - N_{var})]^{1/2}$.

4.4. Magnetic Measurements

DC Magnetic measurements were performed with a MPMS-XL-7 SQUID magnetometer (Quantum Design, San Diego, CA, USA) with an applied magnetic field of 1000 Oe (0.1 T) in the temperature range 2–300 K on polycrystalline samples of compounds **1**–**3** with masses of 2.961, 15.671 and 2.337 mg, respectively. Isothermal magnetization measurements were performed at 2 K with magnetic fields up to 7 T. AC susceptibility measurements were performed on the same samples with an oscillating magnetic field of 4 Oe at low temperatures in the frequency range 10–10,000 Hz with a Quantum Design PPMS-9 (Quantum Design, San Diego, CA, USA) and with different applied DC fields. Susceptibility data were corrected for the sample holders and for the diamagnetic contribution of the salts using Pascal's constants [80].

4.5. Infrared Spectrospcopy

FT-IR spectra were performed on KBr pellets and collected with an Equinox 55 spectrometer (Bruker, Billerica, MA, USA). The spectra of compounds **1** and **2** and the band assignation are reported in the Supporting Information (Figure S17 and Table S2).

5. Conclusions

We have successfully synthesized and characterized two novel two-dimensional anilato-based compounds with single-ion and field-induced single-ion magnet behaviours. Compounds $[Dy_2(C_6O_4H_2)_3(dmso)_2(H_2O)_2]\cdot2dmso\cdot18H_2O$ (**1**) and $[Dy_2(C_6O_4Cl_2)_3(dmso)_4]\cdot2dmso\cdot2H_2O$ (**2**) present distorted hexagonal honeycomb lattices where each Dy(III) ion is connected to other three Dy(III) ions by bis-bidentate anilato bridges. Compound **1** is the first example of this kind of lattice (phase IIb) with $dhbq^{2-}$ whereas compound **2** is the first example of phase IIb with Dy(III) and chloranilato.

Compounds **1** and **2**, as well as the related compound $[Dy_2(C_6O_4(CN)Cl)_3(dmso)_6]$ (**3**), reported by Mercuri et al. [61], show slow relaxation of the magnetization. Compound **1** shows SIM behaviour even when no DC field is applied that seems to relax following a quantum tunnelling mechanism. When a DC field is applied the relaxation of the magnetization in **1–3** follows Orbach and direct mechanisms with U_{eff} in the range 17.1–31.5 K.

In compounds **1**, **2** and **4**, we observe an almost linear dependence of the Ln τ_0 and U_{eff} with the electronegativity of the X group of the anilato ligand and with the distortion of the TDD-8 coordination geometry of the Dy(III) ion.

The series of compounds here reported represents the second series prepared with Dy(III) and different anilato ligands and show that the use of anilato-type ligands with Dy(III) is an adequate strategy to prepare layered SIMs and FI-SIMs that may contain different coordinated and crystallization solvent molecules in the interlayer space and in the hexagonal channels that run perpendicular to the layers. The capacity, already demonstrated in similar systems [33], to evacuate and exchange these solvents opens the possibility to prepare two-dimensional MOFs with SIM behaviour and solvent exchange properties. Another interesting possibility offered by these compounds is the chemical or electrochemical reduction of some, or all, the anilato bridges in order to increase the magnetic coupling, as already observed in some anilato-bridged Dy(III) dimers [81,82], that may eventually lead to a 2D ferrimagnetic order.

Institutional Review Board Statement: Not applicable.

Informed Consent Statement: Not applicable.

Data Availability Statement: The data presented in this study are available on request from the corresponding author.

Conflicts of Interest: The authors declare no conflict of interest. The funders had no role in the design of the study; in the collection, analyses, or interpretation of data; in the writing of the manuscript, or in the decision to publish the results.

References

1. Sessoli, R.; Gatteschi, D.; Caneschi, A.; Novak, M.A. Magnetic Bistability in a Metal-Ion Cluster. *Nature* **1993**, *365*, 141–143. [CrossRef]
2. Bagai, R.; Christou, G. The Drosophila of Single-Molecule Magnetism: $[Mn_{12}O_{12}(O_2CR)_{16}(H_2O)_4]$. *Chem. Soc. Rev.* **2009**, *38*, 1011–1026. [CrossRef]
3. Ishikawa, N.; Sugita, M.; Ishikawa, T.; Koshihara, S.Y.; Kaizu, Y. Lanthanide Double-Decker Complexes Functioning as Magnets at the Single-Molecular Level. *J. Am. Chem. Soc.* **2003**, *125*, 8694–8695. [CrossRef]
4. Sessoli, R.; Powell, A.K. Strategies towards Single Molecule Magnets Based on Lanthanide Ions. *Coord. Chem. Rev.* **2009**, *253*, 2328–2341. [CrossRef]
5. Rinehart, J.D.; Long, J.R. Exploiting Single-Ion Anisotropy in the Design of f-Element Single-Molecule Magnets. *Chem. Sci.* **2011**, *2*, 2078–2085. [CrossRef]
6. Liddle, S.T.; van Slageren, J. Improving f-Element Single Molecule Magnets. *Chem. Soc. Rev.* **2015**, *44*, 6655–6669. [CrossRef] [PubMed]
7. Goodwin, C.A.P.; Ortu, F.; Reta, D.; Chilton, N.F.; Mills, D.P. Molecular Magnetic Hysteresis at 60 Kelvin in Dysprosocenium. *Nature* **2017**, *548*, 439–442. [CrossRef]
8. Liu, J.L.; Chen, Y.C.; Tong, M.L. Symmetry Strategies for High Performance Lanthanide-Based Single-Molecule Magnets. *Chem. Soc. Rev.* **2018**, *47*, 2431–2453. [CrossRef] [PubMed]
9. Yoo, J.; Wernsdorfer, W.; Yang, E.C.; Nakano, M.; Rheingold, A.L.; Hendrickson, D.N. One-Dimensional Chain of Tetranuclear Manganese Single-Molecule Magnets. *Inorg. Chem.* **2005**, *44*, 3377–3379. [CrossRef]
10. Lecren, L.; Roubeau, O.; Coulon, C.; Li, Y.G.; Le Goff, X.F.; Wernsdorfer, W.; Miyasaka, H.; Clerac, R. Slow Relaxation in a One-Dimensional Rational Assembly of Antiferromagnetically Coupled [Mn₄] Single-Molecule Magnets. *J. Am. Chem. Soc.* **2005**, *127*, 17353–17363. [CrossRef]
11. Lin, P.; Gorelsky, S.; Savard, D.; Burchell, T.J.; Wernsdorfer, W.; Clerac, R.; Murugesu, M. Synthesis, Characterisation and Computational Studies on a Novel One-Dimensional Arrangement of Schiff-Base Mn-3 Single-Molecule Magnet. *Dalton Trans.* **2010**, *39*, 7650–7658. [CrossRef] [PubMed]
12. Haryono, M.; Kalisz, M.; Sibille, R.; Lescouezec, R.; Fave, C.; Trippe-Allard, G.; Li, Y.; Seuleiman, M.; Rousseliere, H.; Balkhy, A.M.; et al. One Dimensional Assembly of Mn₆ Single Molecule Magnets Linked by Oligothiophene Bridges. *Dalton Trans.* **2010**, *39*, 4751–4756. [CrossRef] [PubMed]
13. Tsai, H.; Yang, C.; Wernsdorfer, W.; Huang, S.; Jhan, S.; Liu, M.; Lee, G. Mn-4 Single-Molecule-Magnet-Based Polymers of a One-Dimensional Helical Chain and a Three-Dimensional Network: Syntheses, Crystal Structures, and Magnetic Properties. *Inorg. Chem.* **2012**, *51*, 13171–13180. [CrossRef]
14. Dhers, S.; Feltham, H.L.C.; Clerac, R.; Brooker, S. Design of One-Dimensional Coordination Networks from a Macrocyclic {3d-4f} Single-Molecule Magnet Precursor Linked by $[W(CN)_8]^{3-}$ Anions. *Inorg. Chem.* **2013**, *52*, 13685–13691. [CrossRef]
15. Ghosh, S.; Ida, Y.; Ishida, T.; Ghosh, A. Linker Stoichiometry-Controlled Stepwise Supramolecular Growth of a Flexible Cu₂Tb Single Molecule Magnet from Monomer to Dimer to One-Dimensional Chain. *Cryst. Growth Des.* **2014**, *14*, 2588–2598. [CrossRef]
16. Li, R.; Liu, Q.; Wang, Y.; Liu, C.; Liu, S. Evolution from Linear Tetranuclear Clusters into One-Dimensional Chains of Dy(III) Single-Molecule Magnets with an Enhanced Energy Barrier. *Inorg. Chem. Front.* **2017**, *4*, 1149–1156. [CrossRef]
17. Dey, A.; Das, S.; Kundu, S.; Mondal, A.; Rouzieres, M.; Mathoniere, C.; Clerac, R.; Narayanan, R.S.; Chandrasekhar, V. Heterometallic Heptanuclear $[Cu_5Ln_2]$ (Ln = Tb, Dy, and Ho) Single-Molecule Magnets Organized in One-Dimensional Coordination Polymeric Network. *Inorg. Chem.* **2017**, *56*, 14612–14623. [CrossRef]
18. Long, Q.; Hu, Z.; Wang, H.; Yin, C.; Chen, Y.; Song, Y.; Zhang, Z.; Xia, B.; Pan, Z. Field-Induced Single Molecule Magnet Behavior of a $Dy^{III}Na^{I}$ One-Dimensional Chain Extended by Acetate Ions. *Inorg. Chem. Commun.* **2018**, *98*, 127–131. [CrossRef]
19. Zhong, L.; Chen, W.; Li, X.; Ouyang, Z.; Yang, M.; Zhang, Y.; Gao, S.; Dong, W. Four Dinuclear and One-Dimensional-Chain Dysprosium and Terbium Complexes Based on 2-Hydroxy-3-Methoxybenzoic Acid: Structures, Fluorescence, Single-Molecule-Magnet, and Ab Initio Investigation. *Inorg. Chem.* **2020**, *59*, 4414–4423. [CrossRef] [PubMed]

20. Peng, G.; Chen, Y.; Li, B. One-Dimensional Lanthanide Coordination Polymers Supported by Pentadentate Schiff-Base and Diphenyl Phosphate Ligands: Single Molecule Magnet Behavior and Photoluminescence. *New J. Chem.* **2020**, *44*, 7270–7276. [CrossRef]

21. Hojorat, M.; Al Sabea, H.; Norel, L.; Bernot, K.; Roisnel, T.; Gendron, F.; Guennic, B.L.; Trzop, E.; Collet, E.; Long, J.R.; et al. Hysteresis Photomodulation Via Single-Crystal-to-Single-Crystal Isomerization of a Photochromic Chain of Dysprosium Single-Molecule Magnets. *J. Am. Chem. Soc.* **2020**, *142*, 931–936. [CrossRef] [PubMed]

22. Miyasaka, H.; Nakata, K.; Lecren, L.; Coulon, C.; Nakazawa, Y.; Fujisaki, T.; Sugiura, K.; Yamashita, M.; Clerac, R. Two-Dimensional Networks Based on Mn-4 Complex Linked by Dicyanamide Anion: From Single-Molecule Magnet to Classical Magnet Behavior. *J. Am. Chem. Soc.* **2006**, *128*, 3770–3783. [CrossRef]

23. Jeon, I.; Ababei, R.; Lecren, L.; Li, Y.; Wernsdorfer, W.; Roubeau, O.; Mathoniere, C.; Clerac, R. Two-Dimensional Assembly of [(Mn$_2$Mn$_2$^{II})-Mn^{III}] Single-Molecule Magnets and [Cu(Pic)$_2$] Linking Units (Hpic = Picolinic Acid). *Dalton Trans.* **2010**, *39*, 4744–4746. [CrossRef]

24. Kachi-Terajima, C.; Mori, E.; Eiba, T.; Saito, T.; Kanadani, C.; Kitazawa, T.; Miyasaka, H. Mn(III) Salen-Type Single-Molecule Magnet Fixed in a Two-Dimensional Network. *Chem. Lett.* **2010**, *39*, 94–95. [CrossRef]

25. Katsenis, A.D.; Inglis, R.; Prescimone, A.; Brechin, E.K.; Papaefstathiou, G.S. Two-Dimensional Frameworks Built from Single-Molecule Magnets. *Crystengcomm* **2012**, *14*, 1216–1218. [CrossRef]

26. Liu, Y.; Chen, Z.; Ren, J.; Zhao, X.; Cheng, P.; Zhao, B. Two-Dimensional 3d-4f Networks Containing Planar Co$_4$Ln$_2$ Clusters with Single-Molecule-Magnet Behaviors. *Inorg. Chem.* **2012**, *51*, 7433–7435. [CrossRef] [PubMed]

27. Alexandru, M.; Visinescu, D.; Shova, S.; Lloret, F.; Julve, M.; Andruh, M. Two-Dimensional Coordination Polymers Constructed by [Ni^{II}Ln^{III}] Nodes and [W^{IV}(Bpy)(CN)$_6$]$^{2-}$ Spacers: A Network of [(NiDy^{III})-Dy^{III}] Single Molecule Magnets. *Inorg. Chem.* **2013**, *52*, 11627–11637. [CrossRef]

28. Dey, A.; Das, S.; Palacios, M.A.; Colacio, E.; Chandrasekhar, V. Single-Molecule Magnet and Magnetothermal Properties of Two-Dimensional Polymers Containing Heterometallic [Cu$_5$Ln$_2$] (Ln = Gd^{III} and Dy^{III}) Motifs. *Eur. J. Inorg. Chem.* **2018**, 1645–1654. [CrossRef]

29. Kachi-Terajima, C.; Eiba, T.; Ishii, R.; Miyasaka, H.; Kodama, Y.; Saito, T. Spin Ice-Like Magnetic Relaxation of a Two-Dimensional Network Based on Manganese(III) Salen-Type Single-Molecule Magnets. *Angew. Chem. Inter. Ed.* **2020**, *59*, 22048–22053. [CrossRef]

30. Chen, Q.; Li, J.; Meng, Y.; Sun, H.; Zhang, Y.; Sun, J.; Gao, S. Tuning Slow Magnetic Relaxation in a Two-Dimensional Dysprosium Layer Compound through Guest Molecules. *Inorg. Chem.* **2016**, *55*, 7980–7987. [CrossRef]

31. Zhang, J.; Man, Y.; Liu, W.; Liu, B.; Dong, Y. A Dy$_2$ Dimer Derived from a Two-Dimensional Network with a High U$_{eff}$ Value. *Dalton Trans.* **2019**, *48*, 2560–2563. [CrossRef] [PubMed]

32. Huang, L.; Zhang, Y.; Liu, Z.; Wang, X.; Zhao, X.; Yang, E. Two Isostructural Layered Lanthanide(III) Complexes: Syntheses, Structures, Magnetic and Luminescent Properties. *Z. Anorg. Allg. Chem.* **2020**, *646*, 282–287. [CrossRef]

33. Benmansour, S.; Hernández-Paredes, A.; Mondal, A.; López Martínez, G.; Canet-Ferrer, J.; Konar, S.; Gómez-García, C.J. Slow Relaxation of the Magnetization, Reversible Solvent Exchange and Luminescence in 2D Anilato-Based Frameworks. *Chem. Commun.* **2020**, *56*, 9862–9865. [CrossRef] [PubMed]

34. Mondal, A.; Roy, S.; Konar, S. Remarkable Energy Barrier for Magnetization Reversal in 3D and 2D Dysprosium-Chloranilate-Based Coordination Polymers. *Chem. Eur. J.* **2020**, *26*, 8774–8783. [CrossRef]

35. Zakrzewski, J.J.; Chorazy, S.; Nakabayashi, K.; Ohkoshi, S.; Sieklucka, B. Photoluminescent Lanthanide(III) Single-Molecule Magnets in Three-Dimensional Polycyanidocuprate(I)-Based Frameworks. *Chem. Eur. J.* **2019**, *25*, 11820–11825. [CrossRef]

36. She, S.; Gu, X.; Yang, Y. Field-Induced Single Molecule Magnet Behavior of a Three-Dimensional Dy(III)-Based Complex. *Inorg. Chem. Commun.* **2019**, *110*, 107584. [CrossRef]

37. Fordham, S.; Wang, X.; Bosch, M.; Zhou, H. Lanthanide Metal-Organic Frameworks: Syntheses, Properties, and Potential Applications. *Struct. Bond.* **2015**, *163*, 1–27.

38. Wang, C.; Liu, X.; Keser Demir, N.; Chen, J.P.; Li, K. Applications of Water Stable Metal-Organic Frameworks. *Chem. Soc. Rev.* **2016**, *45*, 5107–5134. [CrossRef]

39. Liu, X.; Fu, W.; Bouwman, E. One-Step Growth of Lanthanoid Metal-Organic Framework (MOF) Films Under Solvothermal Conditions for Temperature Sensing. *Chem. Commun.* **2016**, *52*, 6926–6929. [CrossRef] [PubMed]

40. Gómez-Claramunt, P.; Benmansour, S.; Hernández-Paredes, A.; Cerezo-Navarrete, C.; Rodríguez-Fernández, C.; Canet-Ferrer, J.; Cantarero, A.; Gómez-García, C.J. Tuning the Structure and Properties of Lanthanoid Coordination Polymers with an Asymmetric Anilato Ligand. *Magnetochemistry* **2018**, *4*, 6.

41. Artizzu, F.; Atzori, M.; Liu, J.; Mara, D.; Van Hecke, K.; Van Deun, R. Solution-Processable Yb/Er 2D-Layered Metallorganic Frameworks with High NIR-Emission Quantum Yields. *J. Mater. Chem. C* **2019**, *7*, 11207–11214. [CrossRef]

42. Ashoka Sahadevan, S.; Monni, N.; Oggianu, M.; Abhervé, A.; Marongiu, D.; Saba, M.; Mura, A.; Bongiovanni, G.; Mameli, V.; Cannas, C.; et al. Heteroleptic NIR-Emitting Yb^{III}/Anilate-Based Neutral Coordination Polymer Nanosheets for Solvent Sensing. *ACS Appl. Nano Mater.* **2020**, *3*, 94–104. [CrossRef]

43. Ashoka Sahadevan, S.; Monni, N.; Abhervé, A.; Marongiu, D.; Sarritzu, V.; Sestu, N.; Saba, M.; Mura, A.; Bongiovanni, G.; Cannas, C.; et al. Nanosheets of Two-Dimensional Neutral Coordination Polymers Based on Near-Infrared-Emitting Lanthanides and a Chlorocyananilate Ligand. *Chem. Mater.* **2018**, *30*, 6575–6586. [CrossRef]

44.   Benmansour, S.; Hernández-Paredes, A.; Gómez-García, C.J. Effect of the Lanthanoid-Size on the Structure of a Series of Lanthanoid-Anilato 2-D Lattices. *J. Coord. Chem.* **2018**, *71*, 845–863. [CrossRef]

45.   Hernández-Paredes, A.; Cerezo-Navarrete, C.; Gómez García, C.J.; Benmansour, S. Slow Relaxation in Doped Coordination Polymers and Dimers Based on Lanthanoids and Anilato Ligands. *Polyhedron* **2019**, *170*, 476–485. [CrossRef]

46.   Kingsbury, C.J.; Abrahams, B.F.; Auckett, J.E.; Chevreau, H.; Dharma, A.D.; Duyker, S.; He, Q.; Hua, C.; Hudson, T.A.; Murray, K.S.; et al. Square Grid Metal-Chloranilate Networks as Robust Host Systems for Guest Sorption. *Chem. Eur. J.* **2019**, *25*, 5222–5234. [CrossRef]

47.   Kitagawa, S.; Kawata, S. Coordination Compounds of 1,4-Dihydroxybenzoquinone and its Homologues. Structures and Properties. *Coord. Chem. Rev.* **2002**, *224*, 11–34. [CrossRef]

48.   Benmansour, S.; Vallés-García, C.; Gómez-Claramunt, P.; Mínguez Espallargas, G.; Gómez-García, C.J. 2D and 3D Anilato-Based Heterometallic M(I)M(III) Lattices: The Missing Link. *Inorg. Chem.* **2015**, *54*, 5410–5418. [CrossRef]

49.   Atzori, M.; Benmansour, S.; Mínguez Espallargas, G.; Clemente-León, M.; Abhervé, A.; Gómez-Claramunt, P.; Coronado, E.; Artizzu, F.; Sessini, E.; Deplano, P.; et al. A Family of Layered Chiral Porous Magnets Exhibiting Tunable Ordering Temperatures. *Inorg. Chem.* **2013**, *52*, 10031–10040. [CrossRef]

50.   Benmansour, S.; Gómez-García, C.J. Heterometallic Anilato-Based Layered Magnets. *Gen. Chem.* **2020**, *6*, 190033. [CrossRef]

51.   Atzori, M.; Artizzu, F.; Sessini, E.; Marchio, L.; Loche, D.; Serpe, A.; Deplano, P.; Concas, G.; Pop, F.; Avarvari, N.; et al. Halogen-Bonding in a New Family of Tris(Haloanilato)Metallate(III) Magnetic Molecular Building Blocks. *Dalton Trans.* **2014**, *43*, 7006–7019. [CrossRef]

52.   Benmansour, S.; Gómez-Claramunt, P.; Vallés-García, C.; Mínguez Espallargas, G.; Gómez García, C.J. Key Role of the Cation in the Crystallization of Chiral Tris(Anilato)Metalate Magnetic Anions. *Cryst. Growth Des.* **2016**, *16*, 518–526. [CrossRef]

53.   Abrahams, B.F.; Grannas, M.J.; Hudson, T.A.; Hughes, S.A.; Pranoto, N.H.; Robson, R. Synthesis, Structure and Host-Guest Properties of (Et$_4$N)$_2$[Sn^{IV}Ca^{II}(Chloranilate)$_4$], a New Type of Robust Microporous Coordination Polymer with a 2D Square Grid Structure. *Dalton Trans.* **2011**, *40*, 12242–12247. [CrossRef]

54.   Benmansour, S.; Gómez-García, C.J. A Heterobimetallic Anionic 3,6-Connected 2D Coordination Polymer Based on Nitranilate as Ligand. *Polymers* **2016**, *8*, 89. [CrossRef]

55.   Benmansour, S.; Gómez-García, C.J. Lanthanoid-Anilato Complexes and Lattices. *Magnetochemistry* **2020**, *6*, 71. [CrossRef]

56.   Diaz-Torres, R.; Alvarez, S. Coordinating Ability of Anions and Solvents Towards Transition Metals and Lanthanides. *Dalton Trans.* **2011**, *40*, 10742–10750. [CrossRef]

57.   Alvarez, S. Coordinating Ability of Anions, Solvents, Amino Acids, and Gases towards Alkaline and Alkaline-Earth Elements, Transition Metals, and Lanthanides. *Chem. Eur. J.* **2020**, *26*, 8663. [CrossRef]

58.   Abrahams, B.F.; Coleiro, J.; Ha, K.; Hoskins, B.F.; Orchard, S.D.; Robson, R. Dihydroxybenzoquinone and Chloranilic Acid Derivatives of Rare Earth Metals. *J. Chem. Soc. Dalton Trans.* **2002**, 1586–1594. [CrossRef]

59.   Benmansour, S.; Pérez-Herráez, I.; López-Martínez, G.; Gómez García, C.J. Solvent-Modulated Structures in Anilato-Based 2D Coordination Polymers. *Polyhedron* **2017**, *135*, 17–25. [CrossRef]

60.   Benmansour, S.; Pérez-Herráez, I.; Cerezo-Navarrete, C.; López-Martínez, G.; Martínez Hernandez, C.; Gómez-García, C.J. Solvent-Modulation of the Structure and Dimensionality in Lanthanoid-Anilato Coordination Polymers. *Dalton Trans.* **2018**, *47*, 6729–6741. [CrossRef] [PubMed]

61.   Sahadevan, S.A.; Monni, N.; Abhervé, A.; Cosquer, G.; Oggianu, M.; Ennas, G.; Yamashita, M.; Avarvari, N.; Mercuri, M.L. Dysprosium Chlorocyanoanilate-Based 2D-Layered Coordination Polymers. *Inorg. Chem.* **2019**, *58*, 13988–13998. [CrossRef]

62.   Casanova, D.; Llunell, M.; Alemany, P.; Alvarez, S. The Rich Stereochemistry of Eight-Vertex Polyhedra: A Continuous Shape Measures Study. *Chem. Eur. J.* **2005**, *11*, 1479–1494. [CrossRef] [PubMed]

63.   Llunell, M.; Casanova, D.; Cirera, J.; Bofill, J.M.; Alemany, P.; Álvarez, S.; Pinsky, M.; Avnir, D. *Shape*; Version 2.3; University of Barcelona: Barcelona, Spain; Hebrew University of Jerusalem: Jerusalem, Israel, 2013.

64.   Alvarez, S.; Alemany, P.; Casanova, D.; Cirera, J.; Llunell, M. Shape Maps and Polyhedral Interconversion Paths in Transition Metal Chemistry. *Coord. Chem. Rev.* **2005**, *249*, 1693–1708. [CrossRef]

65.   Álvarez, S. Distortion Pathways of Transition Metal Coordination Polyhedra Induced by Chelating Topology. *Chem. Rev.* **2015**, *115*, 13447–13483. [CrossRef]

66.   Zucchi, G.; Thuery, P.; Ephritikhine, M. CSD Communication. Unpublished work. 2012.

67.   Kharitonov, A.D.; Trofimova, O.Y.; Meshcheryakova, I.N.; Fukin, G.K.; Khrizanforov, M.N.; Budnikova, Y.H.; Bogomyakov, A.S.; Aysin, R.R.; Kovalenko, K.A.; Piskunov, A.V. 2D-metal–organic Coordination Polymers of Lanthanides (La(III), Pr(III) and Nd(III)) with Redox-Active Dioxolene Bridging Ligands. *CrystEngComm* **2020**, *22*, 4675–4679. [CrossRef]

68.   Steiner, T. The Hydrogen Bond in the Solid State. *Angew. Chem. Int. Ed.* **2002**, *41*, 48–76. [CrossRef]

69.   Sorace, L.; Gatteschi, D. *Electronic Structure and Magnetic Properties of Lanthanide Molecular Complexes*; Layfield, R.A., Murugesu, M., Eds.; Wiley: Hoboken, NJ, USA, 2015; Volume 1, pp. 1–25.

70.   Benmansour, S.; López-Martínez, G.; Canet-Ferrer, J.; Gómez-García, C.J. A Family of Lanthanoid Dimers with Nitroanilato Bridges. *Magnetochemistry* **2016**, *2*, 32. [CrossRef]

71.   Benmansour, S.; Hernández-Paredes, A.; Gómez-García, C.J. Two Dimensional Magnetic Coordination Polymers Formed by Lanthanoids and Chlorocyananilato. *Magnetochemistry* **2018**, *4*, 58. [CrossRef]

72. Long, J.; Basalov, I.V.; Lyssenko, K.A.; Cherkasov, A.V.; Mamontova, E.; Guari, Y.; Larionova, J.; Trifonov, A.A. Synthesis, Structure, Magnetic and Photoluminescent Properties of Dysprosium(III) Schiff Base Single-Molecule Magnets: Investigation of the Relaxation of the Magnetization. *Chem. Asian J.* **2020**, *15*, 2706–2715. [CrossRef]

73. Long, J.; Selikhov, A.N.; Mamontova, E.; Lyssenko, K.A.; Guari, Y.; Larionova, J.; Trifonov, A.A. Synthesis, Structure, Magnetic and Luminescence Properties of Two Dysprosium Single-Molecule Magnets Based on Phenoxide Dye Ligands. *CrystEngComm* **2020**, *22*, 1909–1913. [CrossRef]

74. Dey, A.; Kalita, P.; Chandrasekhar, V. Lanthanide(III)-Based Single-Ion Magnets. *ACS Omega* **2018**, *3*, 9462–9475. [CrossRef] [PubMed]

75. Demir, S.; Zadrozny, J.M.; Long, J.R. Large Spin-Relaxation Barriers for the Low-Symmetry Organolanthanide Complexes Cp*$_2$Ln(BPh$_4$)] (Cp* = pentamethylcyclopentadienyl; Ln = Tb, Dy). *Chem. Eur. J.* **2014**, *20*, 9524–9529. [CrossRef]

76. Atzori, M.; Artizzu, F.; Marchio, L.; Loche, D.; Caneschi, A.; Serpe, A.; Delano, P.; Avarvari, N.; Mercuri, M.L. Switching-on Luminescence in Anilate-Based Molecular Materials. *Dalton Trans.* **2015**, *44*, 15786–15802. [CrossRef]

77. Sheldrick, G.M. Crystal Structure Refinement with SHELXL. *Acta Cryst. C* **2015**, *71*, 3–8. [CrossRef] [PubMed]

78. Sheldrick, G.M. A Short History of SHELX. *Acta Cryst. A* **2008**, *64*, 112–122. [CrossRef]

79. Dolomanov, O.V.; Bourhis, L.J.; Gildea, R.J.; Howard, J.A.K.; Puschmann, H. OLEX2: A Complete Structure Solution, Refinement and Analysis Program. *J. Appl. Cryst.* **2009**, *42*, 339–341. [CrossRef]

80. Bain, G.A.; Berry, J.F. Diamagnetic Corrections and Pascal's Constants. *J. Chem. Educ.* **2008**, *85*, 532–536. [CrossRef]

81. Zhang, P.; Perfetti, M.; Kern, M.; Hallmen, P.P.; Ungur, L.; Lenz, S.; Ringenberg, M.R.; Frey, W.; Stoll, H.; Rauhut, G.; et al. Exchange Coupling and Single Molecule Magnetism in Redox-Active Tetraoxolene-Bridged Dilanthanide Complexes. *Chem. Sci.* **2018**, *9*, 1221–1230. [CrossRef]

82. Reed, W.R.; Dunstan, M.A.; Gable, R.W.; Phonsri, W.; Murray, K.S.; Mole, R.A.; Boskovic, C. Tetraoxolene-Bridged Rare-Earth Complexes: A Radical-Bridged Dinuclear Dy Single-Molecule Magnet. *Dalton Trans.* **2019**, *48*, 15635–15645. [CrossRef]